Article

Kinetic Membrane Model of Outer Hair Cells

Kuni H. Iwasa[1,*]
[1]National Institutes of Health, NIDCD, Bethesda, Maryland

ABSTRACT   The effectiveness of outer hair cells (OHCs) in amplifying the motion of the organ of Corti, and thereby contributing to the sensitivity of mammalian hearing, depends on the mechanical power output of these cells. Electromechanical coupling in OHCs, which enables these cells to convert electrical energy into mechanical energy, has been analyzed in detail using isolated cells using primarily static membrane models. The mechanical output of OHCs was previously evaluated by developing a kinetic theory based on a simplified one-dimensional model for OHCs. Here, a kinetic description of OHCs is extended by using the membrane model, which was used for analyzing in vitro experiments. This theory predicts, for systems without inertial load, that elastic load enhances positive shift of voltage dependence of the membrane capacitance because of turgor pressure. The effect of turgor pressure increases with increasing elastic load. For systems with inertia, the magnitude of mechanical power output could be ~5% higher than the value predicted by the one-dimensional model at the optimal turgor pressure.

SIGNIFICANCE   This work is an attempt to develop a physical model to clarify the mechanism of outer hair cells in performing their role as an amplifier in mammalian hearing. Specifically, this work extends a static model of these cells into a dynamic one to evaluate mechanical power production, which is essential for the function of these cells. It clarifies the assumptions essential for an earlier phenomenological theory, a one-dimensional model. In addition, it describes the effect of turgor pressure on mechanical power generation.

INTRODUCTION

Outer hair cell (OHC) motility, often referred to as electromotility, is essential for the sensitivity, frequency selectivity, and dynamic range of the mammalian ear (1). This motility is piezoelectric (2–5), based on a membrane protein SLC26A5 (prestin) (6), and it is driven by the receptor potential generated by the sensory hair bundle of each cell. Even though the biological role of this motility has been confirmed by replacing it with its nonfunctional mutants (7), the mechanism with which OHC motility plays this role has not been fully clarified.

This problem involves two factors. One is the speed of conformational transitions of prestin, the motile molecule, and the other is the magnitude of the receptor potential, which drives the motile mechanism.

First, prestin's conformational transitions, which are elicited by voltage changes, accompany charge transfers. This charge movement contributes to the membrane current, together with the regular capacitive current of the plasma membrane. Because the conformational transitions depend on the operating point, the resulting capacitance is voltage dependent. For this reason, it is often referred to as nonlinear capacitance. The frequency dependence of nonlinear capacitance gives rather low characteristic frequencies ~15 kHz (8) and 3 kHz (9).

Conformational transitions are also monitored as the current noise spectrum (10). Sealed patches formed on OHCs show a characteristic frequency of 35 kHz, higher than ~15 kHz for nonlinear capacitance (11). This discrepancy suggests different modes of motion. These observations indicate that those characteristic frequencies likely reflect the mechanical relaxation processes rather than the intrinsic transition rates of the motile molecules.

This interpretation is reinforced by cell displacements elicited by voltage waveforms applied through a suction pipette. In one mode of experiments, the frequency range observed was 8.8–6 kHz or lower (9,12). In quasi-isometric conditions, however, the response extends up to 80 kHz (12).

Second, the intrinsic electric circuit of the cell attenuates the receptor potential at auditory frequencies. For the membrane potential to change, an electric current needs to charge up or down the capacitor, which is formed by the plasma membrane. This factor increasingly attenuates the receptor

potential with increasing stimulation frequency, with the roll-off frequency lower than the operational frequency ([13]).

Various hypotheses have been proposed to address the issue of this voltage attenuation ([14–18]). Mechanical load on OHCs is a possible mechanism for reducing the membrane capacitance ([19–23]). Specifically, elastic load reduces nonlinear capacitance ([20]), and inertial load can eliminate the total membrane capacitance near resonance ([21]). Thus, attenuation of the receptor potential can be avoided near resonance frequency.

The compatibility of OHC electromotility with their biological role could be tested by comparing the optimal power production of the cell with power dissipation in the cochlea ([24],[25]). Such an examination was attempted by using a simple model, which describes the mechanical property of the cell only by the length and the axial stiffness (one-dimensional (1D) model of OHCs for brevity) ([20]) and assuming the energy loss due to the shear in the space between the tectorial membrane and the reticular lamina, which is essential for stimulating hair cells. This study showed that electromotility is compatible with their biological role up to 10 kHz ([21]).

This work develops a kinetic theory based on the membrane model ([26]) and examines the physical basis of a more phenomenological treatment ([20]). It also predicts the effect of turgor pressure, which could play a modulatory role. Besides power production, the amplifier gain of OHCs is discussed. This approach could facilitate extension to a more complex theory, in which the motile element has more than two states to account for anion sensitivity and slower relaxation processes ([27–30]).

METHODS

The system

Here, we consider a system in which an OHC has a mechanical load consisting of viscous, elastic, and inertial components ([Fig. 1]; [Table 1]). This model system provides an OHC with the simplest possible environment so that its performance can be examined. The biological role of this cell could be inferred from this examination.

Let us assume that the lateral wall is uniform and that the cell maintains its characteristic cylindrical shape. The latter assumption could be justified for low frequencies, where inertial force is not significant compared with elastic force within the cell. The limit of the validity is examined later in Results and Discussion, after experimental values for material properties are provided.

In addition, we consider movement of this cell in response to small fast changes in the membrane potential, from an equilibrium condition, ignoring metabolic processes that maintained the physiological condition. Changes in pressure, if present, are assumed gradual and therefore have only a modulatory role. The volume of the cell is assumed constant during voltage changes.

Electrical connectivity

Here, we initially assume that the membrane potential of the cell is controlled by an extracellular electrode and an intracellular electrode with low impedance to facilitate the evaluation of the membrane capacitance. Later on, for evaluating the power output of an OHC, the mechanotransducers at the hair bundle will be incorporated. The receptor potential
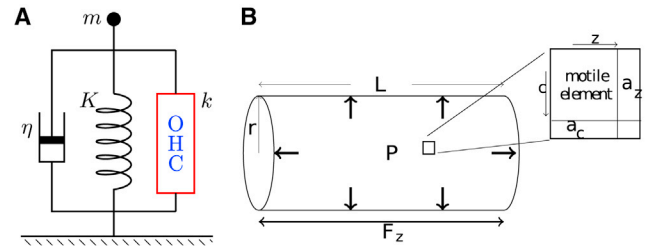

FIGURE 1 The membrane model and mechanical load. (*A*) An OHC (*red rectangle*) is subjected to mechanical load, consisting of viscous η (*left*), elastic K (*middle*), and inertial m (*top*) components. The stiffness of the cell is k. In its lateral membrane, the cell has a membrane protein, which undergoes conformational transitions between two states. (*B*) The membrane model of OHC is shown. The cell body of an OHC is approximated by a cylinder of radius r and length L. Motile elements (*upper right*), which undergo area changes a_z in the axial direction and a_c in the circumferential direction, are uniformly embedded in the cylindrical plasma membrane at density n. The conformational transitions involve transfer of electric displacement q across the membrane. To see this figure in color, go online.

that drives the motile element in the OHCs depends on the membrane capacitance as well as the current source.

Static properties of OHCs

First, consider an OHC in equilibrium. The shape of an OHC is approximated by an elastic cylinder of radius r and length L ([Fig. 1] *B*). Small displacements of the cell can be described by constitutive equations ([31]),

TABLE 1 Parameters of the Membrane Model

Notation	Definition	Value Used	References
d_1	axial modulus	0.046 N/m	(35)
d_2	circumferential modulus	0.068 N/m	(35)
g	cross modulus	0.046 N/m	(35)
a_z	axial area change	-4.5 nm^2	(31)
a_c	circumferential area change	0.75 nm^2	(31)
q	mobile charge	$-0.8\,e$	(2)
n	density of motile element	9×10^{15}/m^2	(31)
r	radius	5 μm	(35)
L_0	cell length	25 μm	
C_0	structural capacitance	10 pF	a
η	drag coefficient	160 nNs/m	(21)

Notation	Meaning	Definition
κ	axial modulus	$d_1 + d_2/4 - g$
k	axial stiffness	$2\pi r\kappa/L_0$
K	elastic load	$2\pi r K_e/L_0$
γ	operating point parameter	$\beta\langle C\rangle(1 - \langle C\rangle)$
ω_r	resonance frequency	$\sqrt{(k+K)/m}$ [b]
ω_η	damping roll-off	$(k+K)/\eta$ [b]
$\overline{\omega}$	reduced frequency	ω/ω_r
a_1	unitary length change	$A/(4\pi r\kappa)$

The definitions of other parameters are $a = -(a_z + 2a_c)$, $A = -(2d_1 - g)a_z + (d_2 - 2g)a_c$, $\varphi = d_1 d_2 - g^2$, $\widehat{K} = K/(k+K)$, $\alpha^2 = 1 + \gamma n(A^2\widehat{K} + \varphi a^2)$, and $\zeta = \gamma Nq^2/C_0$. Of these parameters, $\widehat{K}$, α, and ζ are dimensionless. $i_0\widehat{r}$ is the ac component of transducer current. The parameter values of the motile element reflect that the extended state E is taken as the reference. e, the electronic charge.

[a]The experimentally obtained regular capacitance of an OHC is close to estimates based on the geometrical surface area with the standard value ~1 μF/cm^2 for specific capacitance.

[b]Angular frequency.

$$d_1\varepsilon_z' + g\varepsilon_c' = f_z + \frac{1}{2}rP \qquad (1a)$$

and

$$g\varepsilon_z' + d_2\varepsilon_c' = rP, \qquad (1b)$$

where the first equation is force balance in the axial direction and the second force balance in the circumferential direction. The quantities ε_z' and ε_c' are respectively small elastic strains of the membrane in the axial direction and the circumferential direction. The quantities d_1, d_2, and g are elastic moduli of the membrane in the axial direction, circumferential direction, and cross moduli, respectively; P is the internal pressure, and f_z is the axial tension due to an external force F_z, which can be expressed as $2\pi r f_z$. These elastic moduli assume orthotropy (32,33).

Axial stiffness

The material stiffness k in the axial direction and the axial elastic modulus κ of the cell are expressed as

$$k = \frac{2\pi r}{L_0}\kappa, \qquad (2)$$

where L_0 is the resting length of the cell. The axial modulus κ is obtained as $\kappa = f_z/\varepsilon_z'$ under constant volume condition $\varepsilon_v' = \varepsilon_z' + 2\varepsilon_c' = \mathrm{const.}$, eliminating ε_c' and rP from the constitutive equations (Eq. 1). It can be expressed as (see Appendix A)

$$\kappa = d_1 - g + d_2/4 \qquad (3)$$

This axial stiffness of the cell is material stiffness without a motile element, which would reduce the stiffness in a manner similar to "gating compliance" (31,34).

Motile element

Here, we assume that each motile element undergoes transition between two states, compact (C) and extended (E). In the following, the fraction of the state is expressed in italics.

$$\mathbf{E}(\text{extended}) \quad \rightleftharpoons \quad \mathbf{C}(\text{compact})$$

Unlike conventional description of molecular transitions, we do not assume that transitions between these states take place in accordance with "intrinsic" transition rates. Instead, we assume that transitions between these states are determined by the mechanical constraints in a manner similar to piezoelectricity.

To incorporate the motile element, let us assume that the total strain in the axial direction ε_z and the one in the circumferential direction ε_c consist of elastic components (ε_z' and ε_c') and the contribution of motile elements. Each motile element undergoes electrical displacement q and mechanical displacements a_z and a_c (see Fig. 1 B) during the transition from state E to state C. If the motile elements are uniformly distributed in the lateral membrane at density n, the total strains in the two directions are then respectively expressed by (31)

$$\varepsilon_z = \varepsilon_z' + a_z nC \qquad (4a)$$

and

$$\varepsilon_c = \varepsilon_c' + a_c nC \qquad (4b)$$

The constitutive equations are then rewritten by

$$d_1\varepsilon_z + g\varepsilon_c - (a_z d_1 + a_c g)nC = f_z + \frac{1}{2}rP \qquad (5a)$$

and

$$g\varepsilon_z + d_2\varepsilon_c - (a_z g + a_c d_2)nC = rP \qquad (5b)$$

Notice that the internal pressure P now consists of two components, dependent on the activity of the motile element and independent of it. The latter is referred to as turgor pressure.

In the presence of external elastic load K, axial tension f_z can be expressed by

$$f_z = -K_e\varepsilon_z, \qquad (6)$$

where $K_e = KL_0/(2\pi r)$. Equations 5 and 6 lead to

$$\varepsilon_z = -\frac{AnC - \mu\varepsilon_v}{2(\kappa + K_e)}, \qquad (7)$$

where $A = -(2d_1 - g)a_z + 2\mu a_c$ and $\mu = d_2/2 - g$ (see Appendix A). The quantity ε_v is the volume strain, which can be expressed as $\varepsilon_z + 2\varepsilon_c$ for the cylindrical cell for small strains.

Because the displacement of the cell of our interest is in the auditory frequency range, we assume the cell volume is constant. For this reason, we can regard ε_v as a parameter representative of turgor pressure, which does not depend on the activities of the motile elements and can only change slowly responding to metabolic activity or osmotic pressure.

The axial displacement $Z (= L_0\varepsilon_z)$ of the cell and the total charge of the motile elements Q, respectively, can be expressed using C, the fraction of state C, by

$$Z = -\frac{\pi r}{k + K}(AnC - \mu\varepsilon_v) \qquad (8a)$$

and

$$Q = -qNC, \qquad (8b)$$

where N is the total number of motile elements, i.e., $N = 2\pi r L_0 n$.

Boltzmann distribution

The fraction of state C in equilibrium should be given by a Boltzmann function

$$C_\infty = \exp[-\beta\Delta G]/(1 + \exp[-\beta\Delta G]), \qquad (9)$$

with

$$\Delta G = -q(V - V_0) - a_z f_z - (a_z/2 + a_c)rP, \qquad (10)$$

where ΔG is the energy difference (of state C from state E), V the membrane potential, and $\beta = 1/k_BT$ with Boltzmann's constant k_B and the temperature T. The voltage V_0 determines the operating point. By substituting f_z and rP, we obtain (see Appendix A)

$$\Delta G = -q(V - V_0) + \frac{1}{4\kappa}\left[\left(A^2\widehat{K} + \varphi a^2\right)nC - \left(\mu A\widehat{K} + \varphi a\right)\varepsilon_v\right], \qquad (11)$$

where shorthand notations are

$$a = -(a_z + 2a_c), \tag{12a}$$

$$\widehat{K} = K_e/(\kappa + K_e) = K/(k + K), \tag{12b}$$

and

$$\varphi = d_1 d_2 - g^2 \tag{12c}$$

The volume ε_v is due to turgor pressure P_t. At the extreme hyperpolarization, when the motile element is in the extended state (i.e., C = 0), $P_t = \varepsilon_v \varphi/(2\kappa r)$.

Equation of motion

If $C = C_\infty$, i.e., the distribution of motor states is in equilibrium, the cell does not move. Suppose the membrane potential V changes abruptly; the cell exerts force $k\pi r An(C_\infty - C)$ because a change ΔC in C gives rise to length change $\pi r An\Delta C$ of the cell because of the cylindrical geometry if ε_v is kept constant. Here, k is the material stiffness of the cell defined by Eq. 3. With mechanical load including mass m and drag coefficient η (see Fig. 1 A), the equation of motion can be expressed as

$$m\frac{d^2Z}{dt^2} + \eta\frac{dZ}{dt} = \pi rkAn(C_\infty - C), \tag{13}$$

where C_∞ is the value of C, which satisfies Boltzmann distribution, for the given condition at time t. With the aid of Eq. 8a, this equation can be rewritten in the form

$$m\frac{d^2C}{dt^2} + \eta\frac{dC}{dt} = (k + K)(C_\infty - C), \tag{14}$$

which is intuitive, considering that z is proportional to C. This equation determines the rates of transitions between the two states because C is the only variable, given $C + E = 1$.

This is the same equation derived for the one-dimensional model (20), except that the variable C in this membrane model depends on a larger number of factors, including turgor pressure. The property of the OHC as expressed by the equation cannot be rendered as a simple combination, either series or parallel, of an elastic element and a displacement element.

In the absence of the inertia term, Eq. 14 has a typical relaxation equation for a stochastic process. One may question the inertia term in an equation that describes a stochastic process. It will be shown later that this equation with the inertia term is consistent with the equation of piezoelectric resonance provided that the deviation from equilibrium is small (see Results and Discussion).

Small harmonic perturbation

Because one of the main functions of OHCs is to amplify small signals, the response of OHCs to small harmonic stimulation is of special interest. Assume that the voltage consists of two parts, a constant term $\langle V \rangle$ and small sinusoidal component with angular frequency ω ($= 2\pi f$) and amplitude v:

$$V(t) = \langle V \rangle + v \exp[i\omega t]$$

Then, C and C_∞ should also have two corresponding components

$$C(t) = \langle C \rangle + c \exp[i\omega t] \tag{15}$$

and

$$C_\infty(t) = \langle C_\infty \rangle + c_\infty \exp[i\omega t], \tag{16}$$

and the first-order terms of the equation of motion turn into

$$\left[-(\omega/\omega_r)^2 + i\omega / \omega_\eta + 1 \right]c = c_\infty, \tag{17}$$

with $\omega_r^2 = (k + K)/m$ and $\omega_\eta = (k + K)/\eta$, and

$$c_\infty = \gamma\left[qv + \frac{nc}{2\kappa}\left(A^2\widehat{K} + \varphi a^2\right) \right], \tag{18}$$

with $\gamma = \beta\langle C \rangle(1 - \langle C \rangle)$. Thus, quantity c obeys the equation

$$\left[-(\omega/\omega_r)^2 + i\omega / \omega_\eta + \alpha^2 \right]c = \gamma qv, \tag{19}$$

with $\alpha^2 = 1 + \gamma n(A^2\widehat{K} + \varphi a^2)/(2\kappa)$.

In response to voltage changes, axial displacement Z likewise consists of two components:

$$Z(t) = \langle Z \rangle + z \exp[i\omega t] \tag{20a}$$

and

$$z = -\frac{\pi r}{k + K}Anc \tag{20b}$$

The second equation is derived from Eq. 8a for constant volume strain ε_v.

Nonlinear capacitance

If we express corresponding changes in a similar manner, the charge variable can be expressed as $Q = nq\langle C \rangle + Nqc\exp[i\omega t]$, and nonlinear capacitance C_{nl} is given by

$$C_{nl} = Re[Nqc / v],$$

$$= Re\left[\frac{\gamma Nq^2}{\alpha^2 - \overline{\omega}^2 + i\overline{\omega}/\overline{\omega}_\eta} \right], \tag{21}$$

where $Re[\ldots]$ represents the real part because capacitance is charge transfer synchronous to voltage changes (20). Here, shorthand notations are introduced: $\overline{\omega} = \omega/\omega_r$, $\overline{\omega}_\eta = \omega_\eta/\omega_r$. Nonlinear capacitance can turn negative near resonance frequency and is capable of nullifying the membrane capacitance, as in the case of the 1D model (21) (see Fig. 4 A).

Comparison with one-dimensional model

How do the predictions of the membrane model differ from 1D models? In the following, the 1D model (20,21) is briefly restated to facilitate the comparison.

One-dimensional model

A 1D model has a single parameter k for the cell's elasticity and a single parameter a_1 for mechanical changes of the motile elements. For length changes z and charge transfer Q, the equation that corresponds to Eq. 8a can be written down (20) as

$$Z = \frac{-a_1 kNC}{k + K} \tag{22a}$$

and

$$Q = -qNC, \tag{22b}$$

where C represents the fraction of the compact state, as in the membrane model. The comparison of Eqs. 8a and 22a suggests a_1 corresponds to A. The free energy difference ΔG_1 for the 1D model can be expressed by (20,21)

$$\Delta G_1 = q(V - V_1) + a_1^2 Nk\widehat{K}C \qquad (23)$$

This energy difference ΔG_1 determines $C_\infty = \exp[-\beta\Delta G_1]/(1 + \exp[-\beta\Delta G_1])$ and contributes to the factor $\gamma_1 = \beta\langle C\rangle(1 - \langle C\rangle)$ in the equation of motion. This γ_1 does not depend on turgor pressure—unlike γ, its membrane model counterpart—because ΔG_1 does not have a term that depends on turgor pressure.

The equation for c for the 1D model is

$$\left[-\overline{\omega}^2 + i\overline{\omega}/\overline{\omega}_\eta + \alpha_1^2\right]c = \gamma_1 qv, \qquad (24)$$

with $\alpha_1^2 = 1 + \gamma_1 Na_1^2 k\widehat{K}$, which is independent of turgor pressure.

Nonlinear capacitance

Similar to the derivation of Eq. 21, nonlinear capacitance is given by $Re[Nqc/v]$. Now that c given by Eq. 24, nonlinear capacitance C_{1nl} of the 1D model is expressed by

$$C_{1nl} = Re\left[\frac{\gamma_1 Nq^2}{\alpha_1^2 - \overline{\omega}^2 + i\overline{\omega}/\overline{\omega}_\eta}\right] \qquad (25)$$

which can take negative values near resonance frequency (21).

Correspondence between the two models

The charge transfer q is identical in the two models. The density n of the membrane model is related to N by $n = N/(2\pi rL_0)$. The relationship between the mechanical factors can be obtained by comparing Eq. 22a with Eq. 8a. These two equations, together with Eq. 2, lead to the expression of unitary length change a_1

$$a_1 = \frac{A}{4\pi r\kappa} \qquad (26)$$

Power output and amplifier gain

The analysis above shows that the membrane model and the 1D model lead to similar equations for c. The relation between z and c is the same for both cases because $a_1 kN/(k + K) = An/(\kappa + K_e)$. The difference between the two models originates only from γ and α^2, which, respectively, differ from their counterparts γ_1 and α_1^2 (Table 2). For this reason, the expression for the 1D model will be used in the following with separate definitions for γ and α^2 for the membrane model and their counterparts γ_1 and α_1^2 for the 1D model.

TABLE 2 Correspondence of Parameters in the Membrane Model and in the 1D Model

1D Model	Membrane Model
a_1	$A/(4\pi r\kappa)$
k	$2\pi r\kappa/L_0$
N	$2\pi rL_0 n$
ΔG_1	ΔG
$\alpha_1^2 = 1 + \gamma_1 Na_1^2 k\widehat{K}$	$\alpha^2 = 1 + \gamma n(A^2\widehat{K} + \varphi a^2)/(2\kappa)$

Power output

Under physiological conditions, energy output from an OHC depends on the receptor potential v, which is generated by the transducer current elicited by a relative change $\widehat{r}$ in the hair bundle resistance. This potential depends on the intrinsic circuit property of the cell as well as charge movement due to changes in c, which can be expressed by (20)

$$v = \frac{-i_0\widehat{r} + i\omega Nqc}{\sigma + i\omega C_0}, \qquad (27)$$

where i_0 is the steady state current, σ the conductance of the basolateral membrane, and C_0 the structural membrane capacitance of the hair cell.

The combination of Eqs. 19 and 27 can be written down in the form

$$\left[-\left(\frac{\omega}{\omega_r}\right)^2 + i\omega\left(\frac{1}{\omega_\eta} + \frac{\gamma Nq^2}{\sigma + i\omega C_0}\right) + \alpha^2\right]c = \frac{\gamma i_0 q\widehat{r}}{\sigma + i\omega C_0} \qquad (28)$$

For relatively high frequency, at which ionic currents are overwhelmed by displacement current ωC_0, we obtain

$$c = \frac{\gamma i_0 q\widehat{r}}{i\omega C_0} \times \frac{1}{-\overline{\omega}^2 + i\overline{\omega}/\overline{\omega}_\eta + \alpha^2 + \zeta}, \qquad (29)$$

with $\zeta = \gamma Nq^2/C_0$.

Now, recall that axial displacement z is related to c with Eq. 20b. Energy output from an OHC has two components. One is elastic energy, $(1/2)kz^2$ per half cycle, which is recovered at the end of a cycle. The other is dissipative energy, $(1/2)\eta\omega|z|^2$ per half cycle, which results in power output W, which is given by

$$W(\omega) = \frac{\eta\omega^2}{2\pi}|z|^2$$

$$= \frac{\eta}{2\pi}\left(\frac{k}{k + K}\right)^2\frac{1}{C_0^2}\left|\frac{\gamma a_1 Nqi_0\widehat{r}}{-\overline{\omega}^2 + i\overline{\omega}/\overline{\omega}_\eta + \alpha^2 + \zeta}\right|^2 \qquad (30)$$

Here, the factor $k/(k + K)$ is due to impedance matching. The factors α^2 and ζ introduce turgor pressure dependence. C_0, the structural membrane capacitance, should increase with increasing turgor pressure. This issue will be examined later in Results and Discussion.

Power generation $W(\omega)$ for the membrane model is closely related to its counterpart $W_1(\omega)$ for the 1D model (20,21). The only difference is from the expressions of free energy in the Boltzmann function, resulting in choosing the set γ and α^2 for the membrane model or γ_1 and α_1^2 for the 1D model. Although the membrane model is sensitive to turgor pressure, the 1D model is not.

Amplifier gain

The power gain G of an amplifier is the ratio of output power $W(\omega)$ against input power $W_{in}(\omega)$, where W_{out} is already expressed by Eq. 30 for a given value of $\widehat{r}$, the relative change in the apical membrane resistance due to hair bundle stimulation.

A relative change $\widehat{r}$ in resistance can be associated with a displacement x of hair bundle tip with $\widehat{r} = \widehat{g}x$, where $\widehat{g}$ is the sensitivity of the hair bundle. Because the tips of hair bundles are embedded in the tectorial membrane, the shear between the reticular lamina and the tectorial membrane can also be represented by x. If we can assume that the shear of the subtectorial space x is proportional to the displacement z of the displacement of OHC

cell body, we can put $x = \lambda z$, where λ is a constant. These relationships lead to $x = \hat{r}/(\lambda \hat{g})$ and

$$W_{in}(\omega) = \frac{\eta \omega^2}{2\pi} \left| \frac{\hat{r}}{\lambda \hat{g}} \right|^2 \quad (31)$$

Here, we note that the drag coefficient η consists of two components. One is associated with the movement around the cell that is needed to stimulate the cell. Another is associated with the movement of the hair bundle, for which gating of the transducer channel makes the dominant contribution to drag (36). The drag coefficient η is the same for $W(\omega)$ and $W_{in}(\omega)$ for a given mode of the movement.

The power gain $G(\omega)$ can then be expressed by

$$G(\omega) = \frac{2\pi(\lambda\hat{g})^2}{\eta\omega^2} \times \frac{W(\omega)}{\hat{r}^2} \quad (32a)$$

$$= \frac{1}{\omega_r^2}\left(\frac{k}{k+K}\right)^2\left(\frac{\lambda\hat{g}}{\overline{\omega}C_0}\right)^2 \left| \frac{\gamma a_1 Nqi_0}{-\overline{\omega}^2 + i\overline{\omega}/\overline{\omega}_\eta + \alpha^2 + \zeta} \right|^2 \quad (32b)$$

Equation 32b shows that power gain $G(\omega)$ is a product of two factors. One part depends on the reduced frequency $\overline{\omega} \ (= \omega/\omega_r)$. The other depends on the mechanical resonance frequency ω_r. For a given value of ω_r, the condition $G(\omega) = 1$ may not be satisfied if the mechanical resonance frequency ω_r is too high.

The limiting frequency ω_ℓ, which satisfies $G(\omega_\ell) = 1$, is of special interest because it shows the frequency range in which OHCs can be effective. It has been shown for the 1D model that the frequency ω_ℓ is somewhat higher than the corresponding resonance frequency $\omega_{r,\ell}$ (21).

Amplifier gain at a given location can be related to the limiting frequency ω_ℓ. Let the mechanical resonance frequency at location 2 be ω_{r2}. Then, the amplifier gain $G(\omega_2)$ at that location can be expressed by Eq. 32b, with ω_r replaced by ω_{r2} and $\overline{\omega}$ as ω_2/ω_{r2} instead of $\omega_\ell/\omega_{r,\ell}$.

Then, we have $G(\omega_2) = (\omega_{r,\ell}/\omega_{r2})^2$ if $\eta_2/\omega_{r2} = \eta_\ell/\omega_r$, where ω_2 is the best frequency at location 2. η_2 and η_ℓ are, respectively, the drag coefficients of location 2 and at the location of the limiting frequency. If location 2 is more apical, $\omega_{r2} < \omega_{r,\ell}$, the drag coefficient should satisfy $\eta_2 \leq \eta_\ell$ because the subtectorial gap, which makes a significant contribution to the drag coefficient, is wider for a more apical location. This condition makes the resonance peak sharper at the location. For this reason, the amplifier gain at best frequency ω_2 satisfies $G(\omega_2) > (\omega_{r,\ell}/\omega_{r2})^2$.

Inertia-free condition

In the absence of the inertia term, the power output turns into

$$W(\omega) = \frac{\eta k^2}{2\pi(k+K)^2 C_0^2} \times \frac{(\gamma a_1 Nqi_0\hat{r})^2}{(\omega/\omega_\eta)^2 + (\alpha^2 + \zeta)^2}, \quad (33)$$

which is a monotonically decreasing function of the frequency ω. As Eq. 32a indicates, the power gain $G(\omega)$ is a steeply decreasing function of the frequency ($1/\omega^2$ at low frequencies and $1/\omega^4$ at high frequencies).

Near resonance

For the system with inertia, the power output has a peak

$$W^{(max)} \approx \frac{\gamma\zeta(a_1 Ni_0\hat{r})^2\overline{\omega}_\eta^4}{\alpha^2 + \zeta} \times \frac{\eta k^2}{2\pi(k+K)^2 C_0}, \quad (34)$$

at $\overline{\omega}^2 = \alpha^2 + \zeta - 1/(2\overline{\omega}_\eta^2)$. Because $\alpha^2 > 1$, such a peak exists if $\overline{\omega}_\eta < 1$. However, power production W is a decreasing function of the frequency ω for overdamped systems, in which $\overline{\omega}_\eta$ is large.

These equations for power production are essentially the same as those for the 1D model that has been studied earlier (20,21). The difference is in the definition of α^2 and ζ even though these factors are similar.

RESULTS AND DISCUSSION

Numerical examination

The membrane model and the 1D model lead to parallel expressions for mechanical and electrical displacements, which in turn lead to nonlinear capacitance and power output. The difference in the two stems from the difference in ΔG and ΔG_1. Because the results of the 1D model have been elaborated (21), our focus is whether or not the membrane model leads to different results, using a set of parameter values that have been experimentally determined.

Nonlinear capacitance and factor γ

The operating point factor γ, which contributes to α^2 and ζ, is affected by both turgor pressure and external elastic load through ΔG (see Eq. 10). This sensitivity is reflected in nonlinear capacitance in the low frequency limit (Fig. 2).

Increasing external elastic load broadens the voltage dependence as well as shifts the peak in the positive direction (Fig. 2, A and B). An increase in turgor pressure, represented by ε_v,
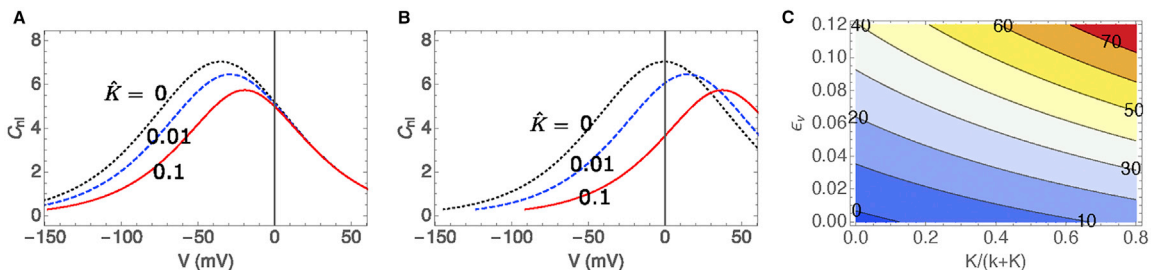

FIGURE 2 Nonlinear capacitance at low frequency. The volume strain ε_v is 0 for (A) and 0.10 for (B). Traces represent elastic load $\hat{K}$ (= $K/(k + K)$): 0 (*dotted, black*), 0.01 (*dashed, blue*), and 0.1 (*red*). (C) Contour plot of peak voltage shift is shown. The abscissa represents $\hat{K}$. The ordinate axis is volume strain ε_v, which represents static turgor pressure. Voltage shifts are color coded (*blue*: negative, *red*: positive), and the values (in mV) are shown in boldface letters in the plot. To see this figure in color, go online.

shifts the peak voltage of nonlinear capacitance in the positive direction. This effect of turgor pressure is consistent with earlier studies, both theoretical (2,31) and experimental (2,37,38). In addition, turgor pressure increases the sensitivity of nonlinear capacitance on the elastic load in both shifting the peak as well as broadening of the dependence (Fig. 2 B). A contour plot of peak voltage shift summarizes the dependence on both turgor pressure and elastic load.

Power output

The power output of an OHC has been described using the 1D model (20,21). Here, we focus on the issue as to how the predictions of the membrane model compare with those of the 1D model for the given set of the parameters.

Inertia-free condition. Under the inertia-free condition, power output is a monotonic decreasing function of frequency as described by Eq. 33. The zero-frequency asymptotes are $\gamma_m/(\alpha_m^2 + \zeta_m)$ for the membrane model and $\gamma_1/(\alpha_1^2 + \zeta_1)$ for the 1D model. The ratio of these zero-frequency asymptotes is plotted in Fig. 3 A.

For high frequencies, the power output declines proportionally to $(1/\omega)^2$. The coefficients are proportional to γ^2. The ratio of the coefficient for the membrane model to that for the 1D model is plotted in Fig. 3 B.

These ratios are very close to unity near $K = k$ (*blue traces*) and deviate significantly for larger elastic load at both ends of the membrane potentials. However, these deviations are not significant near the resting level of the membrane potential (Fig. 3).

The analysis based on the 1D model indicates that the optimal elastic load K to for counteracting viscous drag is $K \approx k$ for physiological operating point near -50 mV (20).

The comparison shows that the power output of the membrane model is similar to that of the 1D model in the physiological membrane potential range. Outside of this voltage range, the membrane model predicts smaller power output than the 1D model. This smaller output is also dependent on the elastic load.

Near resonance

For the 1D model, nonlinear capacitance is negative near resonance frequency (21) and can make the total membrane

capacitance negative (*blue dashed traces* in Fig. 4 A). The frequency of maximal power output (*blue dashed traces* in Fig. 4 B) is close to the frequency of zero capacitance in such cases (*blue traces* in Fig. 4 C).

The membrane model predicts a similar relationship between the membrane capacitance and power output (*red traces* in Fig. 4, A–C are for $\varepsilon_v = 0.065$). Power output predicted by the membrane model is slightly smaller than that of the 1D model for small load. However, the membrane model predicts larger power output for large load K (Fig. 4 D).

The difference between the two stems from the functional forms of ΔG (Eq. 10) and ΔG_1 (Eq. 23). The second term in ΔG has factors that do not exist in ΔG_1. These factors shift the transition point even when $\widehat{K}$ is small.

The ratio W/W_1 of power output predicted by the membrane model to that of the 1D model depends on both turgor pressure and the elastic load (Fig. 4, E and F). The ratio is larger than unity for $\varepsilon_v \approx 0.05$. For both small and large values of ε_v, the ratio decreases with larger load (Fig. 4 E).

For every fixed value of the elastic load, the power output ratio has a broad maximum (Fig. 4 F). The dependence on turgor pressure increases as elastic load increases. The ratio W/W_1 is unity or higher in the range $0.04 < \varepsilon_v < 0.07$. It is larger for larger loads (up to 1.07 for $\widehat{K} = 0.8$). The ratio is lower as load increases outside of this optimal range.

Performance of OHCs

For the 1D model, estimated power output of an OHC is between 0.1 and 10 fW near resonance frequency (21). The effectiveness of OHCs under in vivo conditions was estimated by evaluating a limiting frequency at which the power output of the OHC was equal to the viscous loss, assuming that the major contribution is from the gap between the tectorial membrane and the reticular lamina (25,39,40). This frequency is constrained by two factors, resonance frequency and impedance matching; higher resonance frequency requires stiffer elastic load, which leads to poorer impedance matching for power transfer. This evaluation led to the limit of ~10 kHz if OHC is directly associated with the motion of the basilar membrane (21). To support higher frequencies, OHCs need to be associated to smaller
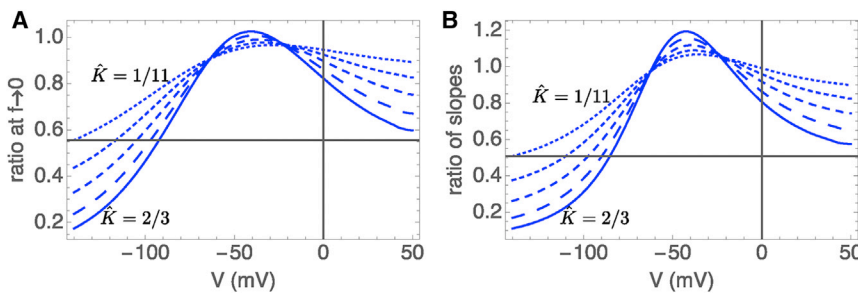

FIGURE 3 Ratio of coefficients for power output of this membrane model to those of the 1D model. (A) The ratio of power output of the membrane model to that of the 1D model at the zero-frequency asymptote is shown. (B) The ratio at high frequencies is shown. Traces correspond to $\widehat{K} = 1/11$ (*dotted*), 1/5 (*short dashes*), 1/3 (*medium dashes*), 1/2 (*long dashes*), and 2/3 (*full line*). To see this figure in color, go online.

elastic load and smaller mass, requiring multiple modes of motion in the organ of Corti (21). The slightly larger (~5%) power output predicted by the membrane model leads to a slightly higher limiting frequency.

The role of turgor pressure

The predicted dependence of power output of OHC on turgor pressure (Fig. 4 D) raises a number of interesting questions. What is the range of turgor pressure in vivo? How much turgor pressure can change? Can it function as a control parameter of the cochlear function?

Power output has a plateau with respect to ε_v at about $\varepsilon_v =$ 0.05 (Fig. 4 F), which corresponds to a static axial strain of $\varepsilon_z = -0.018$ under load-free conditions. This strain is ~36% of the maximal amplitude of electromotility (5% of the cell length). The corresponding turgor pressure is 0.14 kPa. It is probable that the physiological turgor pressure could be lower than this value, as is often the case for biological functions. Such an operating condition allows gain control by the parameters.

However, turgor pressure is not a simple control parameter of power output because changes in turgor pressure accompany shifts of the operating voltage (see, e.g., Fig. 2), even though its effect on the maximal power output could be as large as 50% for large elastic load (Fig. 4 F).

Validity of the cylindrical model

It was assumed in the beginning that the cylindrical shape of the cell is maintained as the cell is driven by changes in the membrane potential and undergoes deformation. The conservation of the cylindrical shape of the cell during motion of the OHC requires that the elastic force of the membrane exceeds the inertial force of the internal fluid. Let x be the amplitude of the end-to-end displacement of a cylindrical cell of radius r and length L. This condition can be expressed by

$$2\pi r\kappa \frac{x}{L} \gg \rho\pi r^2 x\omega^2 x, \tag{35}$$

where κ is the elastic modulus of the cell (in the axial direction), ρ the density of the internal fluid, and ω the angular frequency. The inequality can be expressed by defining a frequency ω_{bal}, at which these two factors are balanced, as

$$\omega \ll \omega_{bal} \equiv \sqrt{\frac{2\kappa}{\rho rxL}} \tag{36}$$

This expression is intuitive in that a smaller displacement, a decrease in cellular dimension, and an increase in the elastic modulus favor the elastic force over the inertial force.

The experimentally obtained value for $2\pi r\kappa$ is 510 nN per unit strain, and it is reasonable to use the density of water (10^3 kg/m^3) for the density ρ. The radius r is 5 μm and

the length L 10 μm for a basal cell. If we assume the amplitude x is 1 nm, an approximate magnitude under in vivo condition, the limit can be expressed by the linear frequency

$$f_{bal} = 4 \times 10^6 \text{Hz} \tag{37}$$

~40 times higher than ~100 kHz for high frequency mammals such as bats and dolphins. The condition is even more favorable for more apical cells because f_{bal} decreases with regard to the square root of $1/L$, whereas the best frequency decreases much more steeply.

This means we can reasonably assume that relative motion of the internal fluid against the plasma membrane can be ignored and that the main mode of cell deformation is elongation and contraction while keeping the cylindrical shape.

The inertia term

The derivation of the equation of motion (Eq. 17) may not appear legitimate in that it introduces the inertia term to a stochastic equation. However, it turns out to be consistent with a standard expression for the admittance of a piezoelectric system.

The standard expression for the admittance Y_{pe} of a piezoelectric resonator can be (41)

$$Y_{pe}(\omega) = i\omega C_0 + \frac{1}{R + i[\omega L_p - 1/(\omega C_p)]}, \tag{38}$$

using an equivalent electric circuit with inductance L_p and resistance R. That implies the correspondence to mechanical resonance system $\omega_r^2 = 1/(C_p L_p)$ and $\omega_\eta = 1/(RC_p)$, leading to

$$Y_{pe}(\omega) = i\omega C_0 + \frac{iC_p}{i\omega/\omega_\eta + 1 - (\omega/\omega_r)^2} \tag{39}$$

Equation 39 is equivalent to Eq. 19 because $Y_{nl} = i\omega Nqc$, and the zero-frequency limit indicates $C_p = \gamma nq^2$ and $\alpha = 1$, which corresponds to $K = 0$ because the external spring does not exist for the piezoelectric element.

This comparison also illustrates a limit of validity for the equation of motion (Eq. 14). Although Eq. 39 for standard piezoelectricity does not depend on the operating point, Eq. 19 for OHC does through the linearization near the equilibrium condition though the operating point factor γ ($= \beta\langle C\rangle(1 - \langle C\rangle)$). The equation of motion Eq. 14 is valid only within a small range of the membrane potential, in which linearization can be justified.

Turgor pressure dependence of C_0

Even though the ratio W/W_1 evaluated is independent of C_0, turgor pressure dependence of C_0 is important for power
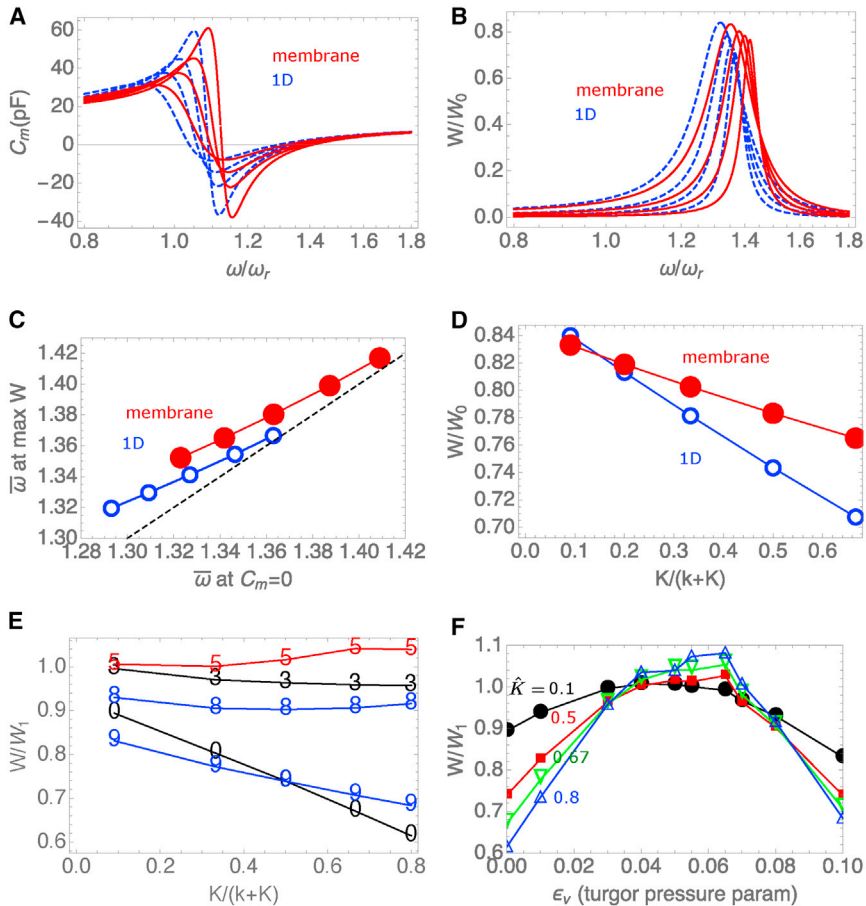
FIGURE 4 The membrane capacitance and the power output of an OHC. (*A*) The membrane capacitance is plotted against the reduced frequency ω/ω_r. The set of plots is generated by increasing the external elastic load K. The values of K correspond to 0.1k, 0.5k, k, and 2k (from the *left* to *right*). Solid red: membrane model. Dashed blue: 1D model. (*B*) Power output function is plotted against frequency. The set of plots are generated by increasing K in a manner similar to (*A*). (*C*) Frequency of maximal power output against the frequency of zero membrane capacitance is shown. The value of K corresponds to, from left to right, 0.1k, 0.25k, 0.5k, k, and 2k. The broken black line indicates equal frequency. (*D*) Power output based on the membrane model (W: *solid red circles*) and on the 1D model (W_1: *open blue circles*) is plotted against $\widehat{K}$ ($= K/(k + K)$). $W_0 = \eta(a_1 N q i o \widehat{r})^2/(2\pi\, C_0^2)$. (*E* and *F*) Ratio of power output of the membrane model to that of the 1D model is shown. (*E*) Dependence on the elastic load $\widehat{K}$ is given. The numbers in the ascending order correspond to $\varepsilon_v = 0$ (labeled 0, *black*), 0.03 (3, *black*), 0.05 (5, *red*), 0.08 (8, *blue*), and 0.1 (9, *blue*). (*F*) Dependence on the volume strain ε_v is shown. $\widehat{K} = 0.1$ (*solid black circles*), 0.5 (*solid red squares*), 0.67 (*open green upside-down triangles*), and 0.8 (*open blue triangles*). In (*A*)–(*D*), $\varepsilon_v = 0.065$. The drag factor ω_η/ω_r is assumed to be 5 at $\widehat{K} = 0$. To see this figure in color, go online.

production W. To my knowledge, experimental data are unavailable, presumably because of the technical difficulty in subtracting voltage-dependent nonlinear components from the total membrane capacitance.

The cylindrical model (Fig. 1 *B*) predicts, for our set of values for elastic moduli, the ratio $\varepsilon_s/\varepsilon_v$ of surface strain to volume strain is ~0.5 (see Appendix D in the Supporting Materials and Methods). If we assume that membrane thickness decreases with an area increase so that the membrane volume is held constant, the relative increase of C_0 is twice the area increase. It is similar to the increase of ε_v. Thus, for a small change of volume strain $\Delta\varepsilon_v$, the resulting change ΔW in power production can be expressed as $\Delta W/W \approx -2\Delta\varepsilon_v$.

It is likely that OHCs have some turgor pressure to maintain their shape as well as their efficiency in power production. If we could assume that the resting value of ε_v is 0.05, power output at $\varepsilon_v = 0.1$ is 10% lower and at $\varepsilon_v = 0$ is 10% higher than the standard value as evaluated in an earlier section.

Drag coefficient

Drag is critical for power balance. It has three sources. One is the shear between the tectorial membrane and the reticular

lamina (21,39,42). Another is the rest of the organ of Corti and the interior of the tectorial membrane because of their deformability (43). This treatment ignores this component because it is hard to evaluate. The third source is gating of the transducer channel in the hair bundle (36). The issue of drag within an OHC and at its outside surface is discussed in Appendices B and C in the Supporting Materials and Methods.

The drag coefficient due to the shear between the tectorial membrane and the reticular lamina is 160 nNs/m per OHC (21). The drag coefficient of the frog hair bundle is 340 nNs/m for gating of nearly all channels in the bundle (36). It would be reasonable to assume that for low stimulation intensity, the contribution of channel gating to the drag coefficient is less than 20 nNs/m, smaller than the gap drag, even though experimental values are unavailable for an OHC hair bundle.

CONCLUSIONS

The membrane model predicts nonlinear capacitance, cell displacement, and power output of OHCs relevant to in vivo conditions. In addition, these predictions are testable by in vitro experiments.

Nonlinear capacitance is sensitive to both turgor pressure and external elastic load. An increased elastic load reduces the peak height and broadens the voltage dependence of nonlinear capacitance. The peak voltage shifts in the positive direction with increasing turgor pressure and elastic load. That is intuitive because increasing internal pressure positively shifts the capacitance peak.

Power output depends on turgor pressure. The optimal power output is expected at $\varepsilon_v \sim 0.06$. Under this condition, for $\widehat{K} \geq 0.5$, the maximal power output is at least 5% higher than the estimate based on the 1D model. However, power output is lower outside of the optimal range of turgor pressure, particularly with larger elastic load.

The membrane model confirms the main predictions of the 1D model; a single mode of vibration of the organ of Corti can be supported up to ~10 kHz but, to cover the entire auditory range, cannot be supported without multiple modes of motion in the cochlear partition (21). This prediction appears consistent with recent observations with optical techniques in that the organ of Corti shows multiple modes of motion (44–46).

APPENDIX A: DERIVATIONS OF ϵ_z AND ΔG

The constitutive equations are given by Eq. 5:

$$d_1\varepsilon_z + g\varepsilon_c - (a_z d_1 + a_c g)nC = f_z + \frac{1}{2}rP,$$

$$g\varepsilon_z + d_2\varepsilon_c - (a_z g + a_c d_2)nC = rP.$$

For a cylindrical cell of length L and radius r, the cell volume is given by $V = \pi r^2 L$. For small length strains, ε_z in the axial direction and ε_c in the circumferential direction, the volume strain ε_v can be expressed by

$$\varepsilon_v = \varepsilon_z + 2\varepsilon_c \qquad (A1)$$

By eliminating the circumferential strain ε_c from these equations, we obtain

$$(2d_1 - g)\varepsilon_z + g\varepsilon_v - 2(a_z d_1 + a_c g)nC = 2f_z + rP \quad (A2a)$$

and

$$\left(g - \frac{d_2}{2}\right)\varepsilon_z + \frac{d_2}{2}\varepsilon_v - (a_z g + a_c d_2)nC = rP \qquad (A2b)$$

By eliminating rP from Eq. A2, an expression for ε_z can be obtained. Then, by replacing ε_z in Eq. A2b with this expression, we obtain an expression for rP. They are

$$2\kappa\varepsilon_z = -AnC + \mu\varepsilon_v + 2f_z \qquad (A3a)$$

and

$$2\kappa rP = -\varphi anC + \varphi\varepsilon_v - 2\mu f_z \qquad (A3b)$$

with shorthand notations

$$A = -\nu a_z + 2\mu a_c, \mu = d_2/2 - g,$$
$$a = -(a_z + 2a_c), \nu = 2d_1 - g, \text{ and} \qquad (A4)$$
$$\varphi = d_1 d_2 - g^2, \kappa = d_1 + d_2/4 - g.$$

Notice here that the parameters A and a are defined such that they are positive. In the absence of the motile elements in the membrane, Eq. A3a is reduced to $f_z = -\kappa\varepsilon_z$. This implies that κ is the axial elastic modulus. See Eqs. 2 and 3.

In the presence of external elastic load, $f_z = -K_e\varepsilon_z$. Then, Eq. A3a turns into

$$2(\kappa + K_e)\varepsilon_z = -AnC + \mu\varepsilon_v, \qquad (A5)$$

where $\widehat{K} = K_e/(\kappa + K_e)$. By substituting f_z in Eq. A3b with $-K_e\varepsilon_z$ using Eq. A6, we obtain

$$2\kappa rP = -\left(\mu A\widehat{K} + \varphi a\right)nC + \left(\mu^2\widehat{K} + \varphi\right)\varepsilon_v \qquad (A6)$$

Notice that Eq. A6 is the same as Eq. 7 in the main text.

With the aid of Eq. A6, the axial stress f_z can be expressed as

$$f_z = \frac{1}{2}\widehat{K}\left(AnC - \mu\varepsilon_v\right) \qquad (A7)$$

The free energy ΔG of state C referenced from state E is given by

$$\Delta G = -q(V - V_0) - a_z f_z - (a_c + a_z/2)rP \qquad (A8)$$

where qV_0 is a constant term. Because $q < 0$ and $a_c + a_z/2 < 0$, both depolarization and increased turgor pressure lead to a decrease of state C. By substituting rP and f_z in Eq. A8 with Eqs. A6 and A7, respectively, we obtain

$$\Delta G = -q(V - V_0) + \frac{1}{4\kappa}\Big[$$
$$\times \left(A^2\widehat{K} + \varphi a^2\right)nC - \left(\mu A\widehat{K} + \varphi a\right)\varepsilon_v\Big], \qquad (A9)$$

which is Eq. 11 in the main text.

SUPPORTING MATERIAL

ACKNOWLEDGMENTS

REFERENCES

1. Liberman, M. C., J. Gao, …, J. Zuo. 2002. Prestin is required for electromotility of the outer hair cell and for the cochlear amplifier. *Nature.* 419:300–304.

2. Iwasa, K. H. 1993. Effect of stress on the membrane capacitance of the auditory outer hair cell. *Biophys. J.* 65:492–498.

3. Mountain, D. C., and A. E. Hubbard. 1994. A piezoelectric model of outer hair cell function. *J. Acoust. Soc. Am.* 95:350–354.

4. Gale, J. E., and J. F. Ashmore. 1994. Charge displacement induced by rapid stretch in the basolateral membrane of the guinea-pig outer hair cell. *Proc. Biol. Sci.* 255:243–249.

5. Dong, X. X., M. Ospeck, and K. H. Iwasa. 2002. Piezoelectric reciprocal relationship of the membrane motor in the cochlear outer hair cell. *Biophys. J.* 82:1254–1259.

6. Zheng, J., W. Shen, …, P. Dallos. 2000. Prestin is the motor protein of cochlear outer hair cells. *Nature.* 405:149–155.

7. Dallos, P., X. Wu, …, J. Zuo. 2008. Prestin-based outer hair cell motility is necessary for mammalian cochlear amplification. *Neuron.* 58:333–339.

8. Gale, J. E., and J. F. Ashmore. 1997. An intrinsic frequency limit to the cochlear amplifier. *Nature.* 389:63–66.

9. Santos-Sacchi, J., and W. Tan. 2018. The frequency response of outer hair cell voltage-dependent motility is limited by kinetics of prestin. *J. Neurosci.* 38:5495–5506.

10. Iwasa, K. H. 1997. Current noise spectrum and capacitance due to the membrane motor of the outer hair cell: theory. *Biophys. J.* 73:2965–2971.

11. Dong, X., D. Ehrenstein, and K. H. Iwasa. 2000. Fluctuation of motor charge in the lateral membrane of the cochlear outer hair cell. *Biophys. J.* 79:1876–1882.

12. Frank, G., W. Hemmert, and A. W. Gummer. 1999. Limiting dynamics of high-frequency electromechanical transduction of outer hair cells. *Proc. Natl. Acad. Sci. USA.* 96:4420–4425.

13. Housley, G. D., and J. F. Ashmore. 1992. Ionic currents of outer hair cells isolated from the guinea-pig cochlea. *J. Physiol.* 448:73–98.

14. Dallos, P., and B. N. Evans. 1995. High-frequency outer hair cell motility: corrections and addendum. *Science.* 268:1420–1421.

15. Mistrík, P., C. Mullaley, …, J. Ashmore. 2009. Three-dimensional current flow in a large-scale model of the cochlea and the mechanism of amplification of sound. *J. R. Soc. Interface.* 6:279–291.

16. Spector, A. A., W. E. Brownell, and A. S. Popel. 2003. Effect of outer hair cell piezoelectricity on high-frequency receptor potentials. *J. Acoust. Soc. Am.* 113:453–461.

17. Rabbitt, R. D., S. Clifford, …, W. E. Brownell. 2009. Power efficiency of outer hair cell somatic electromotility. *PLoS Comput. Biol.* 5:e1000444.

18. Johnson, S. L., M. Beurg, …, R. Fettiplace. 2011. Prestin-driven cochlear amplification is not limited by the outer hair cell membrane time constant. *Neuron.* 70:1143–1154.

19. Ó Maoiléidigh, D., and A. J. Hudspeth. 2013. Effects of cochlear loading on the motility of active outer hair cells. *Proc. Natl. Acad. Sci. USA.* 110:5474–5479.

20. Iwasa, K. H. 2016. Energy output from a single outer hair cell. *Biophys. J.* 111:2500–2511.

21. Iwasa, K. H. 2017. Negative membrane capacitance of outer hair cells: electromechanical coupling near resonance. *Sci. Rep.* 7:12118.

22. Liu, Y., S. M. Gracewski, and J.-H. Nam. 2017. Two passive mechanical conditions modulate power generation by the outer hair cells. *PLoS Comput. Biol.* 13:e1005701.

23. Rabbitt, R. D. 2020. The cochlear outer hair cell speed paradox. *Proc. Natl. Acad. Sci. USA.* 117:21880–21888.

24. Hudspeth, A. J., Y. Choe, …, P. Martin. 2000. Putting ion channels to work: mechanoelectrical transduction, adaptation, and amplification by hair cells. *Proc. Natl. Acad. Sci. USA.* 97:11765–11772.

25. Wang, Y., C. R. Steele, and S. Puria. 2016. Cochlear outer-hair-cell power generation and viscous fluid loss. *Sci. Rep.* 6:19475.

26. Iwasa, K. H. 2010. Chapter 6. Electromotility of outer hair cells. *In* The Oxford Handbook of Auditory Science volume 1: The Ear. P. A. Fuchs, ed. Oxford University Press, pp. 179–212.

27. Oliver, D., D. Z. He, …, B. Fakler. 2001. Intracellular anions as the voltage sensor of prestin, the outer hair cell motor protein. *Science.* 292:2340–2343.

28. Tunstall, M. J., J. E. Gale, and J. F. Ashmore. 1995. Action of salicylate on membrane capacitance of outer hair cells from the guinea-pig cochlea. *J. Physiol.* 485:739–752.

29. Homma, K., and P. Dallos. 2011. Evidence that prestin has at least two voltage-dependent steps. *J. Biol. Chem.* 286:2297–2307.

30. Santos-Sacchi, J., and L. Song. 2014. Chloride-driven electromechanical phase lags at acoustic frequencies are generated by SLC26a5, the outer hair cell motor protein. *Biophys. J.* 107:126–133.

31. Iwasa, K. H. 2000. Effect of membrane motor on the axial stiffness of the cochlear outer hair cell. *J. Acoust. Soc. Am.* 107:2764–2766.

32. Iwasa, K. H. 2001. A two-state piezoelectric model for outer hair cell motility. *Biophys. J.* 81:2495–2506.

33. Tolomeo, J. A., and C. R. Steele. 1995. Orthotropic piezoelectric properties of the cochlear outer hair cell wall. *J. Acoust. Soc. Am.* 97:3006–3011.

34. Howard, J., and A. J. Hudspeth. 1988. Compliance of the hair bundle associated with gating of mechanoelectrical transduction channels in the bullfrog's saccular hair cell. *Neuron.* 1:189–199.

35. Iwasa, K. H., and M. Adachi. 1997. Force generation in the outer hair cell of the cochlea. *Biophys. J.* 73:546–555.

36. Bormuth, V., J. Barral, …, P. Martin. 2014. Transduction channels' gating can control friction on vibrating hair-cell bundles in the ear. *Proc. Natl. Acad. Sci. USA.* 111:7185–7190.

37. Kakehata, S., and J. Santos-Sacchi. 1995. Membrane tension directly shifts voltage dependence of outer hair cell motility and associated gating charge. *Biophys. J.* 68:2190–2197.

38. Adachi, M., M. Sugawara, and K. H. Iwasa. 2000. Effect of turgor pressure on outer hair cell motility. *J. Acoust. Soc. Am.* 108:2299–2306.

39. Allen, J. B. 1980. Cochlear micromechanics–a physical model of transduction. *J. Acoust. Soc. Am.* 68:1660–1670.

40. Hemmert, W., U. Dürig, …, D. Freeman. 2003. A life-sized, hydrodynamical, micromechanical inner ear. *In* Biophysics of the Cochlea: from Molecules to Models. A. Gummer, ed. World Scientific, pp. 409–416.

41. Ikeda, T. 1990. Fundamentals of Piezoelectricity. Oxford University Press, Oxford, UK.

42. Prodanovic, S., S. Gracewski, and J.-H. Nam. 2015. Power dissipation in the subtectorial space of the mammalian cochlea is modulated by inner hair cell stereocilia. *Biophys. J.* 108:479–488.

43. Ghaffari, R., A. J. Aranyosi, and D. M. Freeman. 2007. Longitudinally propagating traveling waves of the mammalian tectorial membrane. *Proc. Natl. Acad. Sci. USA.* 104:16510–16515.

44. Gao, S. S., R. Wang, …, J. S. Oghalai. 2014. Vibration of the organ of Corti within the cochlear apex in mice. *J. Neurophysiol.* 112:1192–1204.

45. He, W., D. Kemp, and T. Ren. 2018. Timing of the reticular lamina and basilar membrane vibration in living gerbil cochleae. *eLife.* 7:e37625.

46. Cooper, N. P., A. Vavakou, and M. van der Heijden. 2018. Vibration hotspots reveal longitudinal funneling of sound-evoked motion in the mammalian cochlea. *Nat. Commun.* 9:3054.